



HAL
open science

Biomass Gasification in an Innovative Spouted-Bed Solar Reactor: Experimental Proof of Concept and Parametric Study

Quentin Bellouard, Stéphane Abanades, Sylvain Rodat

► **To cite this version:**

Quentin Bellouard, Stéphane Abanades, Sylvain Rodat. Biomass Gasification in an Innovative Spouted-Bed Solar Reactor: Experimental Proof of Concept and Parametric Study. *Energy & Fuels*, 2017, 31 (10), pp.10933-10945. 10.1021/acs.energyfuels.7b01839 . hal-02567237

HAL Id: hal-02567237

<https://hal.science/hal-02567237>

Submitted on 12 May 2020

HAL is a multi-disciplinary open access archive for the deposit and dissemination of scientific research documents, whether they are published or not. The documents may come from teaching and research institutions in France or abroad, or from public or private research centers.

L'archive ouverte pluridisciplinaire **HAL**, est destinée au dépôt et à la diffusion de documents scientifiques de niveau recherche, publiés ou non, émanant des établissements d'enseignement et de recherche français ou étrangers, des laboratoires publics ou privés.

Biomass gasification in an innovative spouted-bed solar reactor: experimental proof of concept and parametric study

Quentin Bellouard^{a,b}, Stéphane Abanades^{a*}, Sylvain Rodat^b

^a Processes, Materials and Solar Energy Laboratory, PROMES-CNRS, 7 Rue du Four Solaire, 66120 Font-Romeu, France

^b Univ. Grenoble Alpes INES BP 332, 50 avenue du Lac Léman, F-73375 Le-Bourget-du-lac, France
CEA-LITEN Laboratoire des Systèmes Solaires Haute Température (LSHT), F-38054 Grenoble, France

**Corresponding author: Tel +33 (0)4 68 30 77 30*

E-mail address: stephane.abanades@promes.cnrs.fr

Abstract

Solar thermochemical gasification of lignocellulosic biomass promises a new path for the production of alternative fuels as well as storage and transport of solar energy as a convertible and transportable fuel. The use of concentrated solar energy as the external heat source for the high-temperature reaction allows producing high-value syngas with both higher energy conversion efficiency and reduced cost of gas cleaning and separation, while saving biomass feedstock. A newly designed solar reactor based on the principle of spouted bed reactor was used for continuous solar-driven gasification of biomass particles. The reliable operation of this 1.5 kW reactor was experimentally demonstrated under real solar irradiation using a parabolic dish solar concentrator. Several types of biomass particles were continuously fed in the reactor at temperatures ranging from 1100°C to 1400°C. The injected particles consisted of beech wood or a mix of resinous wood with size ranging from 0.3 mm to 2 mm. The aim

of this study was to achieve a proof of concept for the novel solar reactor applied to biomass gasification. A parametric study of the gasification conditions was realized to optimize the syngas production. The influence of temperature, oxidizing agent nature (H₂O or CO₂) and flow rate, heating configuration (direct or indirect irradiation), biomass type, particles size and feeding rate on gas yield and composition was investigated. The syngas yield increased drastically with the temperature for both steam and CO₂ gasification, while increasing the steam content favored H₂ and reduced CO production. Maximum amounts of produced syngas over 70 mmol/g_{biomass} and carbon conversion rates over 90% were achieved. The biomass energy content was solar-upgraded by a factor of 1.10 at 1400°C.

Introduction

With the fossil fuel resource depletion and the growing concerns about climate change, renewable energies, and particularly biomass, are considered with a growing interest. Biomass presents the advantage of being environmentally clean and available worldwide. A promising and sustainable way to draw benefits from this resource is the thermochemical gasification of biomass as it produces a high quality syngas suitable for power generation or biofuel synthesis.

Through a complex process involving hundreds of chemical species and thousands of reactions, biomass gasification intends to produce a syngas composed of hydrogen and carbon monoxide only. The first step is the pyrolysis of the biomass, which occurs at temperatures above 300°C. During this phase the wood is decomposed into volatile products either condensable (steam and primary tars) or non-condensable gases (H₂, CO, CO₂, CH₄ and C₂H_x), and a solid residue called char. The quantity of char and tars produced can be reduced with higher temperatures and heat transfer rates^{1,2}. The tars are then cracked to produce more gas as well as secondary and tertiary tars. The char is gasified using an oxidizing agent, H₂O or CO₂, to produce syngas according to the following reactions:



Boudouard equilibrium:



Many reactions occur in the gas phase and the main ones are the following:

Water-gas shift reaction:



Steam methane reforming:



Dry methane reforming:



The wood molecular formula can be written approximately as $C_6H_9O_4$ ³, thus in the specific case of wood gasification, the whole process can be represented by the following equation for gasification with H_2O and CO_2 :



The ideal syngas composition can only be obtained if the thermodynamic equilibrium above 900°C is reached. In the case of a real gasification process, higher temperatures will be preferable as they reduce the gas residence time required to reach the thermodynamic equilibrium⁴. Besides, biomass gasification is a very endothermic process and requires a massive energy input. To provide this energy input, two different kinds of technologies have been developed⁵, namely autothermal and allothermal reactors. The first one uses both the heat and H_2O and CO_2 obtained from the combustion of a part of the biomass feedstock (at least 30%) to sustain the process and to gasify the rest of the feedstock. The second one relies on an external heat source for the process needs. In this context, the use of concentrated solar power to provide the necessary heat to the reaction is a promising way to save biomass or fossil resources and it has already been investigated⁶⁻⁸. Thanks to the absence of combustion, a solar process produces a syngas with a higher calorific value and no combustion

product contamination. Besides, this also eliminates the need for upstream air separation and reduces costly downstream gas cleaning and separation requirements. The whole feedstock being gasified, the syngas output per unit of feedstock is increased. Thanks to the use of highly concentrated solar power, higher gasification temperatures ($>1200^{\circ}\text{C}$) are reachable thus improving the reaction kinetics and the syngas quality and greatly reducing the tar content. This process thus represents an efficient way to store the solar energy in a chemical form and improves the dispatchability of the initial resource.

Several solar reactors have already been designed for carbonaceous materials gasification, the most represented concepts being packed bed and fluidized bed solar reactors. They can be classified into two categories, (i) directly irradiated solar reactors (windowed) allowing optimal radiative transfer to the feedstock and (ii) indirectly irradiated solar reactors offering the possibility to remove the window at the expense of an additional heat transfer resistance through an opaque heat transfer wall serving as absorber and heat conductor.

Regarding packed bed solar reactors, either they are directly or indirectly irradiated, the core is the same. They consist of a cavity receiver filled with a batch of feedstock which receives the concentrated solar power directly through a window⁹⁻¹¹ or indirectly through an emitter plate re-emitting energy via IR radiation^{12, 13}. Such reactors offer high reaction extent thanks to the presence of a large quantity of feedstock particles absorbing the radiation and the long solid residence time. Those reactors can also accept a large variety of feedstock with different compositions and large particle sizes. However the scaling up of those reactors is limited for the same reason, the thermal inertia of the bed leads to an important temperature gradient and non-homogenous reactions, thus impacting the reaction rate and the syngas quality¹². To avoid such problem, fluidized bed solar reactors were proposed in which the feedstock is continuously stirred with inert particles by a neutral gas and/or the oxidizing agent. Several concepts of solar fluidized bed reactors have already been tested^{10, 14-22}, however the proper operation of those reactors requires small particle sizes (<1 mm) with preliminary shredding and sorting steps for the feedstock. For both packed and fluidized bed solar reactors, no suitable concept was proposed for continuous gasification process. Indirectly irradiated entrained flow solar reactors were developed for continuous gasification process with horizontal²³ or vertical²⁴

circulation of the particles. Because of the short particle residence times in those reactors, the particle sizes must be limited and only feedstock with high reactivity can be gasified. Even so the short residence time of particles and gas has an adverse impact on carbon conversion rate and syngas composition. In order to offer both long residence time and continuous process, some alternative concepts were developed. One of them is based on the principle of an indirectly irradiated drop-tube reactor combined with a packed bed. A tubular cavity receives the solar irradiation while a porous material in the heated zone retains the particles until their complete gasification while allowing the gas to pass through ²⁵⁻²⁸. Another alternative concept is a directly irradiated horizontal cylinder in which the feedstock and the gas are injected in a way to form a vortex flow inside the reactor, thus extending the residence time of the particles inside the heated zone ²⁹⁻³². This reactor was recently modified into an indirectly irradiated reactor and the two configurations were compared ³³.

This study follows an experimental campaign realized with a drop tube/packed bed reactor ²⁸ and focuses on the parametric study of a newly developed solar reactor under real solar irradiation, based on the concept of spouted bed reactor. Spouted bed reactors have already been used for non-solar biomass pyrolysis and gasification ³⁴⁻³⁶ and present the advantages to offer a high solid residence time as well as a continuous stirring of the feedstock. However, previously developed reactors show different characteristics and operating principles. For example, packed-bed ^{12,13} and fluidized bed ²⁰⁻²² reactors were chiefly operated in batch as the reacting particles were preloaded in the reactor before heating and most reactors used artificial light instead of concentrated solar radiation. In this study, the developed solar-heated reactor also offers the possibility to continuously feed the reactant and to work with both directly and indirectly irradiated modes thanks to a removable emissive plate. Such continuous operation with particles injection directly at high temperatures represents a major innovation when compared with previous reactors. Finally, in previous works ²², the fluidized bed was mostly heated from the top surface with high radiation losses and temperature gradient through the bed from top to bottom (also the case for packed beds ^{12,13}). The new developed reactor in this study features a cavity receiver with a small aperture on top to maximize energy absorption while minimizing radiation losses, thereby achieving homogeneous temperatures inside the cavity.

The concept validation, experimental demonstration and performance assessment of the solar reactor was conducted under real solar irradiation.

Experimental section

Feedstock

Several feedstocks were used for the experiments to assess the impact of the wood composition and particles size on syngas production and biomass injection. While the biomasses are all grinded wood, they present some differences in composition, humidity content, low heating value (LHV) and particles size. The characteristics of the four different types of feedstocks are presented in Table 1.

Experimental set-up

The entire experimental system is depicted in Figure 1. It is mainly composed of a solar concentrating system, the 1.5 kW solar reactor associated with a particle feeding system, a filtering unit and a gas analysis unit. The reactor is located at the 6th floor to the south of the CNRS-PROMES building (Odeillo, France), in a room above ground as described in Figure 2. A sun tracking heliostat located 30 m below the trapdoor reflects the solar radiation vertically to a parabolic mirror (2 m diameter). This parabolic mirror then concentrates the flux on the focal point (2 cm diameter) where the reactor aperture is settled. The flux density at the focal point is up to 10 MW/m² (for a Direct Normal Irradiation (DNI) of 1 kW/m²) with a Gaussian distribution. The trapdoor activated via a motor can be partially closed or opened to adjust the incident power and thus the reactor temperature.

The design of the solar reactor is based on the concept of conical spouted bed reactor³⁷, for which the feasibility for biomass gasification has already been proven^{35,36}. The cavity of the reactor, which receives the solar flux and shelters the reaction, is a 78 mm inside diameter cylinder (47 mm height, 3 mm wall thickness) whose bottom is a cone (68 mm height) with a 60° angle, for a total height of 11.5 cm. This cavity is made of a FeCrAl alloy whose melting point is around 1500°C. A gas flow comprising Ar carrier gas (0.3 NL/min) and an oxidizing agent (CO₂ or H₂O) is injected via an

alumina tube (4 mm o.d., 2 mm i.d.) from the bottom of the conical part of the cavity to (i) propel the biomass particles to the top of the cavity where they can absorb highly concentrated solar power, and (ii) ensure proper mixing of the biomass with the oxidizing agent. The trajectory of the biomass particles is schemed in Figure 3.

All the gas flows are injected via mass-flow controllers (model Brooks SLA5850S, scale: 0-5 NL/min, precision: $\pm 0.2\%$ of full scale). Steam is injected via a stainless steel capillary exiting 5 mm below the bottom of the conical cavity and placed inside the gas injection tube, water is vaporized inside the capillary and then entrained by the Ar flow before entering the cavity at the tip of the cone, thus providing continuous steam flow inside the system. The liquid water flow rate is controlled by a mass flow controller (scale 0-30 g/h, precision: $\pm 1\%$ of full scale). To broaden the gas stream with an enlarged effective gas flow diameter and prevent biomass particles from being propelled outside the cavity, a fixed bed (about 15 mm high) of SiC particles (1-2.3 mm diameter), which does not move with the gas flow, is set at the bottom of the cavity. This bottom layer of particles also improves the reactor thermal inertia by absorbing radiation and storing energy, and further protects the bottom injection alumina tube from solid or liquid reaction products clogging.

The cavity is supported by a shaped piece of porous ceramic that ensures a thermal insulation on its side and bottom (~ 30 mm thickness around the cavity). To limit the thermal losses on top of the cavity and infrared re-radiation, an alumina cap with a 20 mm aperture is placed above it. This aperture is positioned at the focal point of the parabolic mirror to maximize the incoming flux. The alumina cap and the top of the insulating ceramic (which are at the same level) are protected by a 2 mm layer of zirconium fiber felt. An additional layer of graphite (2 mm thick) with a 15 mm aperture is placed around the alumina cap aperture to protect the rest from the highly concentrated flux during the adjustment of the reactor position. The stainless steel reactor shell (15 cm i.d., 17 cm o.d.) is water-cooled at the bottom and the sides, and a transparent hemispherical glass window is used to operate in controlled atmosphere. The window is hermetically attached to the shell, thus separating the cavity from the ambient air. An argon protective flow (2 NL/min) is continuously injected inside the window area to prevent it from being soiled by gasification residues. It is also possible to operate the reactor in

an indirectly-irradiated configuration to prevent particle deposition on the window. A graphite plate on top of a SiC plate (2 mm thick) is inserted between the cavity and the alumina cap (17 mm from the aperture) to absorb the solar power and heat the cavity by re-radiation. The graphite plate (not in contact with the oxidant injected in the lower cavity) offers a good protection against thermal shocks and separates the upper cavity receiving solar radiation from the lower cavity receiving biomass feedstock.

The biomass is mechanically injected directly in the cylindrical part of the cavity using a screw feeding device going through the reactor wall and the insulating material. The particles exit the tilted screw feeder and then fall down by gravity inside the cavity where they are gasified thanks to the oxidizing gas injected from the cavity bottom. An Ar flow (1 NL/min) is injected in the hopper in which the biomass is stored (capacity 1.15 L) and then goes through the screw path (screw dimensions: 14 mm o.d., 10 mm core diameter) all the way to the cavity, thus preventing backflow of the hot gases from the cavity up to the screw. Instead the gas exits the reactor via an alumina tube (8 mm o.d., 5 mm i.d.) passing through the insulating material and the reactor wall. This outlet gas comprises the gas products from the gasification reaction occurring in the cavity as well as the carrier gas injected at the bottom, and the protective gas injected both at the window and through the particle feeding system. Then the exiting gas flows into a gas washing unit composed of a bubbler and two cartridge filters (filtration threshold: 99.99998% for 0.1 μm particle size) to be cooled and to separate the remaining steam, ashes and tars before entering the gas analyzer.

Metrology and gas analysis

Temperature inside the cavity was measured at two locations using B-type thermocouples (Pt-Rh). Those thermocouples were covered by an alumina sheath and inserted in the cavity through the insulating ceramic and the reactor shell as shown in Figure 1 (T_2 & T_3). Another B-type thermocouple (T_1) was placed inside the insulating ceramic to measure the temperature of the upper part of the cavity wall. A solar-blind pyrometer (operating at 4.8-5.2 μm in a H_2O absorption band) placed at the center of the parabolic mirror was used to measure the temperature inside the cavity (direct heating configuration) or at the surface of the emissive plate (indirect heating configuration). Three pressure

gauges were used to monitor the pressure in the gas injection tube at the window (P_1), in the cavity (P_2) and in the gas outlet pipe (P_3). The pressure in the cavity was especially controlled during the gasification process to monitor the gas expansion.

An in-line syngas analyzer (GEIT 3100) was used to measure the concentration of the main species in the produced gas. The concentrations of CO, CO₂, CH₄ and C_nH_m are measured using NDIR cells and the H₂ concentration using a thermal conductivity detector. For some experiments the gas was collected in a sampling bag to be analyzed with a gas chromatograph (GC, Varian CP49000) in order to double-check the results. The gas chromatograph and the in-line analyzer showed similar results with a 5% relative error. Only the data from the in-line analyzer are reported here for the data exploitation.

The amount of syngas produced was measured by a volumetric gas counter (drum-type gas meter, Ritter TG20, range 40-2800 NL/h) and calculated from the known Ar flow. The composition and the amount of syngas being known, it was possible to determine its Low Heating Value (LHV). One of the main interests of solar-driven biomass gasification relates to the improvement of the energy content of the initial biomass. A performance indicator used to assess this solar upgrade, called Cold Gas Efficiency (CGE), is the ratio of the solar gasification products energy content (LHV) to the energy content of the initial biomass feedstock and is defined as follows:

$$CGE = \frac{LHV_{syngas} \times m_{syngas}}{LHV_{feedstock} \times m_{feedstock}} \quad (9)$$

A ratio superior to 1 thus indicates an upgrade of the initial biomass energy content through gasification and the efficient storage of solar energy.

The biomass composition being known, it is possible to calculate the carbon conversion rate defined as the ratio of carbon contained in the gaseous product (in the form of CO, CO₂, CH₄ and C_nH_m) to the injected carbon in the biomass.

Experimental protocol and conditions

The reactor was first flushed with inert gas to remove air and then the trapdoor was progressively opened (speed 19 mm/s, 105 s for full opening) in several steps to avoid thermal shocks of the ceramic parts. The reactor was heated up to the targeted temperature inside the cavity with continuous Ar flow (total duration of 30 min to reach 1200°C in the direct heating configuration and 60 min in the indirect heating configuration). The temperature was controlled by adjusting the trapdoor opening. Then the oxidant (either steam or CO₂) was injected at the cavity bottom before starting the continuous biomass particle feeding in the cavity at high temperature. Initially the biomass amount was precisely weighted and preloaded inside the hopper, and the feeding was operated until complete biomass particle load injection (the total amount of feedstock fed during each run was thus precisely known). The particles fall inside the cavity by gravity and are pushed by the upward particles from the screw and by the Ar injected via the screw path along with the particles. The gasification then proceeds inside the cavity where the oxidant (steam or CO₂) is injected (Fig. 3). Because the biomass injection induces a slight temperature decrease in the cavity (energy consumed for particle heating and endothermal reaction), the reactor was initially overheated by about 30-50°C above the temperature set-point. The gas species concentrations at the reactor outlet were analyzed continuously to determine the syngas yield and chemical composition, as well as the total amount of each gas produced by time integration of the production rates. After the test, the different reactor components were cleaned and the remaining char/ash in the cavity and outlet parts (tubes, bubbler, filters) was weighted. After each run, a mass balance was performed from the amounts of solid residues and gas products compared to the initial amounts of injected biomass and gaseous oxidant. The mass balance was closed at over 95% in every case. The gas velocity at the bottom cavity entrance for the spouted bed (mixture of Ar and oxidizing gas) was settled above the minimum spouting gas velocity (2.91 m/s at the exit of the alumina tube for a required minimum gas velocity of roughly 1 m/s at normal conditions). Cold pretests with visual observation of preloaded wood particle movement confirmed the particle lifting and stirring inside the cavity at room temperature, thus providing evidence of the spouting process. However, it is likely that upon continuous particles injection at high temperature, the gasification reaction rate is high enough to consume rapidly and entirely the whole particles during their feeding inside the cavity and that the spouting process may differ from cold tests because of particles

consumption and shrinkage. It thus appears possible that most of the reactions occur fast in the gas volume and that the formation of a bed just comes from the remaining char particles. It was not possible to visually observe the real process of particle movement and gasification inside the reactor because of the harsh temperature conditions.

For this study, all the experiments were conducted with a continuous biomass injection (total amount of 10 g) with a feeding rate set to 2 g/min and using the Type A biomass (unless stated otherwise). However due to some issues with the motor driving the screw feeder and the biomass rheology, the actual biomass feeding rate was somewhat lower and varied between 1 and 2 g/min. All the experiments were carried out using either H₂O or CO₂ as an oxidizing agent. Most of them were realized with an oxidizing agent flow rate such that the biomass/oxidant ratio was close to the stoichiometric ratio presented in equation (7) and (8). The biomass humidity rate was included in the calculation to determine the required oxidant flow rate for both H₂O and CO₂. For a biomass feeding rate of 2 g/min, the calculated stoichiometric flow rates are 234 mg/min for H₂O and 0.29 NL/min for CO₂. Due to the lower actual biomass injection rate, these calculated flow rates were rounded down to 200 mg/min for H₂O and 0.2 NL/min for CO₂. All the parameters of the experiments are presented in Table 2.

Results and discussion

Temperature influence

The influence of the temperature on syngas composition from biomass gasification with H₂O and CO₂ was studied. Injections of biomass (type A) were realized in the reactor heated at 1100°C, 1200°C, 1300°C and 1400°C while injecting either H₂O or CO₂. The quoted nominal temperatures correspond to T₃ measured inside the cavity. As the values given by T₂ and T₃ were very close (less than 10°C discrepancy), the temperature could be considered uniform in the reaction zone where the particles are injected. The quantity of gas produced per gram of dry biomass [mmol/g_{biomass}] during gasification with H₂O at the different temperatures is presented in Figure 4 along with the evolution of

the cold gas efficiency. These gaseous productions are obtained by time integration over an entire run. The theoretical values attained at the thermodynamic equilibrium (TE) reached above 1000°C are also represented. The presence of light hydrocarbons (mainly C₂H₂) was detected in the syngas but in very small quantity (< 0.3 %) and was thus not represented. The mean residence time of the gas inside the cavity is about 0.6±0.1 s at the considered operating conditions (gas flow rates calculated at the actual reactor temperature and pressure). The quantity of produced syngas increases with temperature (Fig. 4) approaching the thermodynamic equilibrium, but it is not reached because of kinetic limitations.

With the increase of the temperature, the quantity of H₂ and CO produced from the same mass of biomass also increases, from 22 and 22.7 mmol/g_{biomass} at 1100°C to 28.9 and 35.8 mmol/g_{biomass} at 1400°C for CO and H₂, respectively. On the opposite, the quantity of CH₄ decreases with the rise of temperature, from 5.2 mmol/g_{biomass} at 1100°C to 3 mmol/g_{biomass} at 1400°C. These variations can be explained by the improvement of the kinetic rate of gasification (Eq. 1) and steam methane reforming (Eq. 5). The quantity of CO₂ produced remains steady between 3.3 and 4.1 mmol/g_{biomass} regardless of the temperature. The H₂/CO ratio reaches a maximum of 1.4 at 1300°C. The overall quantity of gas produced increases with the temperature, but this growth seems to be lowered above 1300°C. It is also interesting to notice that the overall quantity of carbon-containing gas increases with the temperature too, leading to an improvement of the carbon conversion rate from 78.8% at 1100°C to 91.5% at 1400°C. These variations induce an improvement of the cold gas efficiency (CGE) with the rise of the temperature. It appears that the energy content of the syngas exceeds the one of biomass beyond 1250°C, with the CGE reaching a maximum of 1.10 at 1400°C. However this value remains lower than the one obtained at the thermochemical equilibrium mostly because of the production of CO₂ that cannot be valorized during combustion. Independently of the reaction temperature, small amounts of char were observed in the outlet tubes and the filtration devices (less than 0.5 g for 10 g of injected biomass). A small amount of char (< 0.1 g) was also occasionally found in the biomass injection tube at the end of the experiment.

The same experiments were realized with a flow of CO₂ (0.2 NL/min mixed with 0.3 NL/min Ar) as oxidizing agent and the quantity of gas produced per gram of dry biomass is shown in Figure 5

along with the CGE. Those values are also compared to those obtained at the thermodynamic equilibrium. Once again the presence of light hydrocarbons was noted but in low quantities ($< 0.3\%$). The total CO_2 measured by the on-line syngas analyzer at the reactor exit corresponds mainly to the excess of the CO_2 injected as oxidizing agent and the CO_2 produced by the reaction (the only fraction of CO_2 in the evolved syngas related to the reaction cannot be quantified in the case of CO_2 gasification), and CO_2 is thus not represented in Figure 5.

As expected from Eqs. (1) and (2), the quantity of H_2 produced is much lower and the quantity of CO much higher for gasification with CO_2 than for steam gasification, leading to low H_2/CO ratios (ranging from 0.51 to 0.69). However it is interesting to notice that the quantity of H_2 is rather low at 1100°C ($16.6 \text{ mmol/g}_{\text{biomass}}$) while it is almost constant for higher temperatures, reaching a maximum of $25.5 \text{ mmol/g}_{\text{biomass}}$ at 1400°C . As for steam gasification, the quantity of CH_4 decreases with the rise of temperature thanks to the improvement of the CH_4 dry reforming (Eq. 6) reaction rate, ranging from $4.8 \text{ mmol/g}_{\text{biomass}}$ at 1100°C to almost $1.2 \text{ mmol/g}_{\text{biomass}}$ at 1400°C . The temperature has also an influence on the CGE. Compared to steam gasification, the calculated CGE shows a smaller fluctuation range, rising from almost 0.98 at 1100°C up to 1.04 at 1300°C and then stabilizing. Similarly to steam gasification experiments, small amounts of char were found in the outlet tubes and the filtration devices (about 0.8 g for 10 g of injected biomass).

The results obtained here are consistent with those obtained in an indirectly irradiated tubular reactor²⁸.

Comparison of the reactor heating configurations

The indirectly-irradiated reactor configuration was investigated to assess the performances according to the reactor heating concept. The reactor heating is longer for the indirectly-irradiated configuration than for the directly-irradiated configuration because of the presence of the emissive plate. The maximum temperature reached was thus 1200°C (temperature inside the cavity). The Figure 6 presents the evolution of temperature inside the cavity (T_3) during heating phase for both direct and

indirect heating configuration. Temperature below 200°C could not be measured by the thermocouple and the 0 on the time axis corresponds to the moment when the trap door is opened.

It takes less than 35 min to reach 1200°C with direct heating and 52 min to reach 1400°C, which is the maximum operating temperature of the reactor in this configuration. With indirect heating, reaching the maximum operating temperature (1200°C) takes 61 min. Experiments of steam gasification (steam flow rate: 200 mg/min) were carried out at 1100°C, 1150°C and 1200°C with the indirectly-irradiated configuration and compared with the directly-irradiated configuration under the same conditions (Table 3).

The total amount of gas produced (thus carbon conversion rate) is higher for the indirectly-irradiated configuration. As a result, the carbon conversion rate ranges from 78.8% at 1100°C to 83.4% at 1200°C for direct heating, whereas it is improved with indirect heating and goes from 88.1% at 1100°C to 97% at 1200°C. This increase of the amount of produced syngas appears to come from chiefly the increase of the amount of evolved CH₄ at the expense of a lower H₂ production. Regarding CO, the quantities produced are the same for both direct and indirect heating configurations. The quantity of H₂ is slightly lower with indirect heating configuration at 1150°C and 1200°C. The CO₂ quantity is slightly higher for indirect heating, while the CH₄ quantity is much higher for indirect heating. The quantity of produced H₂ is lower with indirect heating configuration, certainly due to the increase of CH₄ production.

The CGE in indirect heating configuration is always higher than 1 and reaches 1.15 at 1200°C chiefly because of the high calorific value of CH₄ contained in the syngas. However the syngas composition is not ideal for a Fisher-Tropsch process due to the important presence of CH₄. This means the particle conversion is enhanced at the expense of a lower syngas quality in the case of indirect heating. It is likely that the favored CH₄ formation is the result of a lower gas residence time in the indirect heating configuration. This could be explained by a different gas flow hydrodynamic inside the cavity. Indeed, the Ar flow injected at the window cannot enter directly the cavity because of the inserted emitter plate in indirect heating configuration. Thus, it goes through the interstitial

space between the cavity and the insulating material to enter the cavity preferably via the bottom and then exits the reactor, thereby increasing the gas velocity inside the cavity and reducing the residence time. This change in the gas flow hydrodynamic might have an adverse impact on the kinetic rate of the gasification process because of a lowered gas residence time. Furthermore, the use of the emissive plate as the heat transfer wall induces additional energy losses and thereby does not allow the reactor to operate above 1200°C, which represents a strong limitation for the gasification process.

Effect of oxidizing agent and stoichiometry

To completely gasify biomass feedstock with steam, a H₂O/biomass molar ratio of 2 or higher is necessary (Eq. 7). The humidity content of the initial biomass feedstocks (Table 1) was included to determine the flow rates and the H₂O/biomass ratio. For this study, two steam flow rates were used (mixed with 0.3 NL/min Ar as carrier gas): 200 mg/min for stoichiometric conditions and 500 mg/min for excess steam conditions (for a biomass feeding rate of 2 g/min, this second steam flow rate would be equivalent to a H₂O/biomass molar ratio of 3.3). The steam was continuously injected even after the end of the biomass injection (10 g of biomass type A) to completely gasify the char.

According to Figure 7, the quantity of CO produced is higher with the lowest steam flow rate, whatever the temperature. In contrast, the quantity of CO₂ produced increases with the steam flow rate due to the excess of oxygen supplied, which favors the formation of CO₂ instead of CO (Water-gas shift (Eq. 4)). Likewise, the higher the steam flow rate, the higher the amount of H₂ produced, thus increasing its proportion in the final syngas. As a result, the H₂/CO ratio is always higher with the highest steam flow rate. At the lowest temperature, the quantity of syngas produced is larger with a lower flow rate, but a reverse trend is observed when increasing the temperature. As a result, the quantity of syngas produced is larger with the highest steam flow rate at 1300°C and the difference becomes significant at 1400°C. At a given temperature, the carbon conversion rate is approximately the same for both steam flow rates, with a maximum of 91.5% at 1400°C. Regarding CH₄, no significant impact of the steam flow rate can be observed. Overall the temperature has a more significant impact on syngas production and composition than the steam flow rate. The maximum

obtained CGE was 1.1 at 1400°C with a steam flow rate of 200 mg/min. At the same temperature but for a steam flow rate of 500 mg/min, the CGE value is quite close and reaches 1.09.

Regarding gasification with CO₂, CO₂ flow rates of 0.2 NL/min (close to the stoichiometry) and 0.6 NL/min were investigated using biomass type A as feedstock. Accounting for the biomass humidity as an oxidant agent, this second CO₂ flow rate corresponds to an oxidant/biomass molar ratio of 3.2. The quantities of syngas produced during experiments at three different temperatures are presented in Figure 8 (CO₂ is not represented because in excess in the feed gas).

The influence of the CO₂ flow rate is much more significant than the influence of the steam flow rate. The increase of the CO₂ flow rate results in enhancing the total amount of syngas produced at a given temperature. The quantity of CO produced strongly increases with the CO₂ flow rate thanks to the gasification of the chars by the CO₂ (Eq. 3). The carbon conversion rate is thus also increased, ranging between 81.1% at 1200°C and 85.2% at 1400°C at the lowest CO₂ flow rate, and between 86.3% at 1200°C and 97.1% at 1400°C at the highest CO₂ flow rate. However, the quantity of H₂ produced decreases sharply when increasing the CO₂ flow rate because of the reverse water-gas shift reaction (Eq. 4). A part of the initial hydrogen content of the biomass is thus converted into steam water (not measured by the gas analyzer) and additional CO is produced. To confirm this statement, thermodynamic equilibrium calculations were realized using the GEMINI software (Gibbs Energy MINImizer) in order to compute the system composition at the equilibrium state (Table 4).

According to the equilibrium composition (Table 4), the formation of H₂O is favored to the detriment of H₂ when an excess of CO₂ is used. The water is condensed in the bubbler after exiting the reactor and it is not detected in the syngas, hence the total quantity of hydrogen in the syngas drops with the increase of the CO₂ flow rate. In the case of gasification with CO₂, hydrogen is brought to the reaction only through the biomass and its humidity content, and it is interesting to notice that the total amount of hydrogen (H) in the syngas (H₂ and CH₄ included) is constant around 56 mmol/g_{biomass} independently of the temperature and varies only with the increase of the inlet CO₂ flow. The total input of hydrogen (H) in the reactor being 77.8 mmol/g_{biomass} (biomass humidity included), a large part of the input hydrogen (28%) seems to react with CO₂ to form H₂O and CO even with the lowest CO₂

flow rate. The amounts of tar and char produced at the end of the experiments were reduced by the increase of the CO₂ flow rate (about 0.3 g for 10 g of injected biomass with 0.6 NL/min of CO₂ flow rate regardless of the temperature).

The type of oxidant is an important parameter influencing the reactor performances. The gasifying agent affects not only the gasification rates but also the syngas composition and the solar upgrade factor. Moreover CO₂ gasification can be a way to valorize CO₂ and it was thus necessary to compare the differences in syngas yield and composition when gasifying with either H₂O or CO₂. The results show drastically different reactor performances according to the type of oxidant. The amount of syngas is higher in the case of steam gasification regardless of the amount of oxidant and temperature. This comes from the ability of steam to react with CO forming CO₂ and H₂. A part of the steam is thus consumed and integrated as H₂ in the syngas. This is even more pronounced with excess steam resulting in higher CO₂ production. Conversely, for CO₂ gasification, the increase of the oxidant amount favors the steam generation that is not included in the syngas, and the CO production is favored over the H₂ production.

Effect of biomass type and particle size

The four different types of biomass (Table 1) were steam gasified with a steam flow rate of 200 mg/min at 1100°C, 1200°C and 1300°C to compare the amounts of gas produced (Figure 9).

The influence of temperature on the syngas production is confirmed for all the biomasses. However, the effect of temperature is less pronounced for the largest particles (type B), which may be more sensitive to heat and mass transfer limitations. Besides, the observed differences in syngas productions are not very significant for the range of particle size studied. The particle size and the temperature influence both the kinetic rate of gasification and the hydrodynamic of the reactor. These parameters are essential to the gasification process as they determine the required reaction duration for complete gasification. However the effect of particle size on the gas-solid flow hydrodynamic in spouted bed reactors is not well studied, especially for the present size of particles³⁸. Moreover, the particle size is

drastically reduced as soon as the biomass is injected in the hot cavity because of the rapid reactions, which explains to a large extent the low sensitivity of the process to the initial particle size. Similar experiments were conducted (except for biomass type C) using CO₂ (0.2 NL/min) as oxidizing agent (Figure 10), confirming again the low sensitivity of syngas yield and composition to the type of biomass and particle size, but the high sensitivity to the temperature.

A steep increase of the syngas production and CGE is obtained when increasing the temperature whatever the type of biomass considered for both steam and CO₂ gasification, but the effect of particle size on the syngas production is negligible. This points out that increasing the particle size (thus reducing the pre-processing costs of the feedstock) is a possible option for future optimization of the process.

Biomass feeding rate influence

For a given solar power input, a trade-off in the biomass feeding rate may exist since a too high feeding rate would cause a drop of the cavity temperature because of insufficient energy input, thus reducing the kinetic rate of the gasification reaction and eventually leading to solid reactant accumulation inside the reactor. On the contrary a too low feeding rate would result in complete conversion but limited syngas production, thereby leading to incomplete utilization of the solar energy input. The effect of the biomass feeding mass flow rate on the syngas quality was thus investigated. A given amount of biomass (10 g of biomass type B) was injected continuously and gasified at 1300°C using steam (200 mg/min) as oxidizing agent. During the first test (Figure 11a), the feeding rate was ~0.65 g/min and the feedstock was completely injected after less than 16 min. For the second test (Figure 11b), a higher feeding rate was used (close to 1 g/min).

Despite a clear difference in the syngas production rate, a similar amount of syngas is produced regardless of the biomass feeding rate (Table 5) and the carbon conversion rate remains identical (80.4%).

However, the amount of each gas and the syngas composition are changed significantly. A higher feeding rate favors H₂ and CO production to the detriment of the other gas species. The higher production of CO₂ at low feeding rate can be explained by the excess of steam with respect to biomass induced by the lower feeding rate of biomass. This induces a higher quantity of CO₂ produced at the expense of the CO production, as previously observed on the effect of oxidizing agent flow rate (Figure 7). With the highest feeding rate the quantity of CH₄ also diminishes, which might explain the increase of H₂ production. The question of the energy efficiency of the reactor is raised. The solar-to-fuel energy conversion efficiency of the reactor represents the fraction of the energy input (both solar and calorific content of feedstock) converted into the chemical energy of the syngas produced. It was increased from 10.2% to 16.5% when increasing the biomass feeding rate from 0.65 to 1 g/min (same total amount injected: 10 g), because the solar energy input was inherently lowered when reducing the injection duration. For 2 g/min of fed biomass (610W of power content), the gas power output would be 671W for a typical CGE of 1.10, yielding an energy conversion efficiency of 32% for the 1.5 kW scale reactor. A low feeding rate reduces the solar-to-fuel energy conversion efficiency, but a too high feeding rate would cause a drop of reactor temperature, thus lowering both the particle conversion to syngas and the syngas quality. Consequently, the reactant feed flow rate must be optimized to match the rate of the chemical reaction. A trade-off may thus exist between maximum allowable amount of injected feedstock and maximum chemical conversion to syngas.

Effect of delayed injection of gasifying agent

Biomass pyrolysis followed by char gasification (delayed oxidizing agent injection) was performed to quantify separately the amount of syngas produced during pyrolysis and gasification phases. Biomass (10 g of type A) was injected at 1300°C during 7 min in Ar atmosphere (pyrolysis step). Once no more gas was produced from the flash pyrolysis, the oxidizing agent (either H₂O or CO₂) was then injected to gasify the char. The time evolution of the syngas composition obtained with steam is shown in Figure 12 and the averaged time-integrated syngas composition in Figure 13a.

The quantities of syngas produced during pyrolysis are lower than those produced during steam gasification (with continuous injection of steam). When steam is injected to gasify char (case of delayed steam injection), a second phase of gas production is observed with an almost equimolar CO and H₂ production (Eq. 1). CH₄ production only occurs during pyrolysis phase. Regarding CO₂, even if a small quantity is produced after delayed steam injection, the total amount of CO₂ produced is smaller than for steam gasification with continuous steam injection (Figure 13a). Moreover, the total quantity of syngas produced is smaller in the case of delayed steam injection. This difference is explained by a lower carbon conversion rate in the case of the delayed steam injection (80%) when compared with continuous gasification (about 85%). The same experiment was realized at 1200°C and similar results and trends were observed (Figure 13b).

A further experiment was carried out at 1300°C using CO₂ and the comparative results for delayed CO₂ injection (0.2 NL/min) and continuous injections (0.2 NL/min and 0.6 NL/min) are represented in Figure 14 and Figure 15. Similarly to delayed steam injection, the production of CH₄ only occurs during pyrolysis phase. This is also the case of H₂ production for delayed CO₂ injection, which denotes that all the hydrogen contained in the biomass is volatilized during the pyrolysis phase. Only CO is produced after delayed CO₂ injection (according to Eq. 3). Regarding the peak of CO production (at time = 14 min) of the continuous CO₂ injection experiment (0.6 NL/min), it is due to the sudden fall of some biomass particles that were stuck at the tip of the screw. The fact that no H₂ is produced at this moment shows that the biomass had already undergone pyrolysis and was reduced to char in the screw. Regarding CH₄, the highest quantity of CH₄ is produced during the experiment with delayed CO₂ injection, as opposed to the case of steam. This is due to the fact that without CO₂, the dry reforming of methane (Eq. 6) cannot occur. In contrast, steam reforming could occur because of the humidity contained in the biomass. Meanwhile, the absence of CO₂ allows reaching a higher production of H₂ because the reverse water-gas shift reaction (Eq. 4) cannot occur. These experiments bring interesting insights into the chemical mechanism of gasification process.

Conclusion

An innovative spouted bed solar reactor was successfully operated for the gasification of wood at high temperature. The influence of each operating parameter on the syngas yield was investigated during continuous injection of given amounts of biomass. The gas yields were improved with the rise of temperature (from 1100°C to 1400°C) and to a lesser extent with the injection of the oxidizing agent (H₂O or CO₂) in over-stoichiometric proportion. The size of the particles did not show any significant impact on the gas yields for the range of particle size considered (0.3 to 2 mm). High carbon conversion rates, up to 97.1 %, were achieved. During this experimental study, a high-quality syngas was produced with a typical energy upgrade factor of 1.10, meaning a 10% improvement of the initial biomass energy content by the solar energy input. The reactor was operated according to different heating modes with either direct heating of the reacting particles or indirect heating via an opaque heat transfer wall. The indirectly-irradiated configuration requires further investigation to reach higher upper operating temperatures and optimize the gas residence time inside the cavity. This parametric study conducted on a new solar reactor concept provides several insights for further optimization, which should be focused on determining the optimal biomass feed mass flow rate and gas flow rate (residence time) to maximize the thermochemical reactor performances during continuous solar operation.

Acknowledgments

This study was financially supported by ADEME (The French Environment and Energy Management Agency) and CEA (French Alternative Energy and Atomic Energy Commission). The study was also partly funded by the Carnot Institute “Energies du Futur” (REACSOL project 2014-2016). The authors thank S. Ravel and M. Grateau for her helpful expertise and support on biomass characterization, P.E. Frayssines and J. Cigna for the manufacturing of the reactor and R. Joubert and O. Prevost for their technical expertise and help during the experimental campaign.

References

- (1) X. Deglise and A. Donnot, "Bois énergie," *Techniques de l'ingénieur*, BE8535, Jul. 2004.
- (2) A. Dufour, P. Girods, E. Masson, Y. Rogaume, and A. Zoulalian, "Synthesis gas production by biomass pyrolysis: Effect of reactor temperature on product distribution," *Int. J. Hydrog. Energy*, vol. 34, no. 4, pp. 1726–1734, Feb. 2009.
- (3) D. Ballerini, *Les biocarburants, état des lieux, perspectives et enjeux du développement*, Éditions Technip ed. Paris: IFP Publications, 2006.
- (4) C. Higman and M. van der Burgt, *Gasification*, 2nd ed. Elsevier, 2008.
- (5) S. Heidenreich and P. U. Foscolo, "New concepts in biomass gasification," *Prog. Energy Combust. Sci.*, vol. 46, pp. 72–95, 2015.
- (6) M. Puig-Arnavat, E. A. Tora, J. C. Bruno, and A. Coronas, "State of the art on reactor designs for solar gasification of carbonaceous feedstock," *Sol. Energy*, vol. 97, pp. 67–84, Nov. 2013.
- (7) A. Nzihou, G. Flamant, and B. Stanmore, "Synthetic fuels from biomass using concentrated solar energy – A review," *Energy*, vol. 42, no. 1, pp. 121–131, Jun. 2012.
- (8) N. Piatkowski, C. Wieckert, A. W. Weimer, and A. Steinfeld, "Solar-driven gasification of carbonaceous feedstock—a review," *Energy Environ. Sci.*, vol. 4, no. 1, pp. 73–82, Dec. 2010.
- (9) D. W. Gregg, R. W. Taylor, J. H. Campbell, J. R. Taylor, and A. Cotton, "Solar gasification of coal, activated carbon, coke and coal and biomass mixtures," *Sol. Energy*, vol. 25, no. 4, pp. 353–364, 1980.
- (10) R. W. Taylor, R. Berjoan, and J. P. Coutures, "Solar gasification of carbonaceous materials," *Sol. Energy*, vol. 30, no. 6, pp. 513–525, 1983.
- (11) M. Flechsenhar and C. Sasse, "Solar gasification of biomass using oil shale and coal as candidate materials," *Energy*, vol. 20, no. 8, pp. 803–810, Aug. 1995.
- (12) N. Piatkowski and A. Steinfeld, "Solar-Driven Coal Gasification in a Thermally Irradiated Packed-Bed Reactor," *Energy Fuels*, vol. 22, no. 3, pp. 2043–2052, 2008.
- (13) N. Piatkowski, C. Wieckert, and A. Steinfeld, "Experimental investigation of a packed-bed solar reactor for the steam-gasification of carbonaceous feedstocks," *Fuel Process. Technol.*, vol. 90, no. 3, pp. 360–366, Mar. 2009.

- (14) J. P. Murray and E. A. Fletcher, "Reaction of steam with cellulose in a fluidized bed using concentrated sunlight," *Energy*, vol. 19, no. 10, pp. 1083–1098, Oct. 1994.
- (15) P. von Zedtwitz and A. Steinfeld, "Steam-Gasification of Coal in a Fluidized-Bed/Packed-Bed Reactor Exposed to Concentrated Thermal Radiation Modeling and Experimental Validation," *Ind. Eng. Chem. Res.*, vol. 44, no. 11, pp. 3852–3861, May 2005.
- (16) R. Müller, P. v. Zedtwitz, A. Wokaun, and A. Steinfeld, "Kinetic investigation on steam gasification of charcoal under direct high-flux irradiation," *Chem. Eng. Sci.*, vol. 58, no. 22, pp. 5111–5119, Nov. 2003.
- (17) Kodama, Y. Kondoh, T. Tamagawa, A. Funatoh, K.-I. Shimizu, and Y. Kitayama, "Fluidized Bed Coal Gasification with CO₂ under Direct Irradiation with Concentrated Visible Light," *Energy Fuels*, vol. 16, no. 5, pp. 1264–1270, Sep. 2002.
- (18) T. Kodama, S. Enomoto, T. Hatamachi, and N. Gokon, "Application of an Internally Circulating Fluidized Bed for Windowed Solar Chemical Reactor with Direct Irradiation of Reacting Particles," *J. Sol. Energy Eng.*, vol. 130, no. 1, pp. 014504–014504, Jan. 2008.
- (19) Kodama, N. Gokon, S. Enomoto, S. Itoh, and T. Hatamachi, "Coal Coke Gasification in a Windowed Solar Chemical Reactor for Beam-Down Optics," *J. Sol. Energy Eng.*, vol. 132, no. 4, pp. 041004–041004, Sep. 2010.
- (20) N. Gokon, R. Ono, T. Hatamachi, L. Liuyun, H.-J. Kim, and T. Kodama, "CO₂ gasification of coal cokes using internally circulating fluidized bed reactor by concentrated Xe-light irradiation for solar gasification," *Int. J. Hydrog. Energy*, vol. 37, no. 17, pp. 12128–12137, Sep. 2012.
- (21) N. Gokon, T. Izawa, T. Abe, and T. Kodama, "Steam gasification of coal cokes in an internally circulating fluidized bed of thermal storage material for solar thermochemical processes," *Int. J. Hydrog. Energy*, vol. 39, no. 21, pp. 11082–11093, Jul. 2014.
- (22) N. Gokon, T. Izawa, and T. Kodama, "Steam gasification of coal cokes by internally circulating fluidized-bed reactor by concentrated Xe-light radiation for solar syngas production," *Energy*, vol. 79, pp. 264–272, Jan. 2015.

- (23) T. Melchior, C. Perkins, P. Lichty, A. W. Weimer, and A. Steinfeld, "Solar-driven biochar gasification in a particle-flow reactor," *Chem. Eng. Process. Process Intensif.*, vol. 48, no. 8, pp. 1279–1287, Aug. 2009.
- (24) P. Lichty, C. Perkins, B. Woodruff, C. Bingham, and A. Weimer, "Rapid High Temperature Solar Thermal Biomass Gasification in a Prototype Cavity Reactor," *J. Sol. Energy Eng.*, vol. 132, no. 1, pp. 011012–011012, Jan. 2010.
- (25) M. Kruesi, Z. R. Jovanovic, E. C. dos Santos, H. C. Yoon, and A. Steinfeld, "Solar-driven steam-based gasification of sugarcane bagasse in a combined drop-tube and fixed-bed reactor – Thermodynamic, kinetic, and experimental analyses," *Biomass Bioenergy*, vol. 52, pp. 173–183, May 2013.
- (26) M. Kruesi, Z. R. Jovanovic, and A. Steinfeld, "A two-zone solar-driven gasifier concept: Reactor design and experimental evaluation with bagasse particles," *Fuel*, vol. 117, Part A, pp. 680–687, Jan. 2014.
- (27) M. Kruesi, Z. R. Jovanovic, A. Haselbacher, and A. Steinfeld, "Analysis of solar-driven gasification of biochar trickling through an interconnected porous structure," *AIChE J.*, vol. 61, no. 3, pp. 867–879, Mar. 2015.
- (28) Q. Bellouard, S. Abanades, S. Rodat, and N. Dupassieux, "Solar thermochemical gasification of wood biomass for syngas production in a high-temperature continuously-fed tubular reactor," *Int. J. Hydrog. Energy*, vol. 42, no. 19, pp. 13486–13497, May 2017.
- (29) A. Z'Graggen, P. Haueter, G. Maag, A. Vidal, M. Romero, and A. Steinfeld, "Hydrogen Production by Steam-Gasification of Petroleum Coke Using Concentrated Solar Power: Reactor Experimentation With Slurry Feeding," *ASME 2006 Int. Sol. Energy Conf.*, pp. 23–27, Jan. 2006.
- (30) A. Z'Graggen, P. Haueter, D. Trommer, M. Romero, J. C. de Jesus, and A. Steinfeld, "Hydrogen production by steam-gasification of petroleum coke using concentrated solar power—II Reactor design, testing, and modeling," *Int. J. Hydrog. Energy*, vol. 31, no. 6, pp. 797–811, May 2006.
- (31) A. Z'Graggen, P. Haueter, G. Maag, A. Vidal, M. Romero, and A. Steinfeld, "Hydrogen production by steam-gasification of petroleum coke using concentrated solar power—III.

- Reactor experimentation with slurry feeding,” *Int. J. Hydrog. Energy*, vol. 32, no. 8, pp. 992–996, Jun. 2007.
- (32) A. Z’Graggen, P. Haueter, G. Maag, M. Romero, and A. Steinfeld, “Hydrogen production by steam-gasification of carbonaceous materials using concentrated solar energy—IV. Reactor experimentation with vacuum residue,” *Int. J. Hydrog. Energy*, vol. 33, no. 2, pp. 679–684, Jan. 2008.
- (33) F. Müller *et al.*, “A pressurized high-flux solar reactor for the efficient thermochemical gasification of carbonaceous feedstock,” *Fuel*, vol. 193, pp. 432–443, Apr. 2017.
- (34) A. R. Fernandez-Akarregi, J. Makibar, G. Lopez, M. Amutio, and M. Olazar, “Design and operation of a conical spouted bed reactor pilot plant (25 kg/h) for biomass fast pyrolysis,” *Fuel Process. Technol.*, vol. 112, pp. 48–56, Aug. 2013.
- (35) A. Erkiaga, G. Lopez, M. Amutio, J. Bilbao, and M. Olazar, “Steam gasification of biomass in a conical spouted bed reactor with olivine and γ -alumina as primary catalysts,” *Fuel Process. Technol.*, vol. 116, pp. 292–299, Dec. 2013.
- (36) A. Erkiaga, G. Lopez, M. Amutio, J. Bilbao, and M. Olazar, “Influence of operating conditions on the steam gasification of biomass in a conical spouted bed reactor,” *Chem. Eng. J.*, vol. 237, pp. 259–267, Feb. 2014.
- (37) M. Olazar, M. J. San Jose, R. LLamosas, and J. Bilbao, “Hydrodynamics of Sawdust and Mixtures of Wood Residues in Conical Spouted Beds,” *Ind. Eng. Chem. Res.*, vol. 33, no. 4, pp. 993–1000, Apr. 1994.
- (38) H. Cui and J. R. Grace, “Spouting of biomass particles: A review,” *Bioresour. Technol.*, vol. 99, no. 10, pp. 4008–4020, Jul. 2008.

Table 1: Dry composition and characteristics of the different biomasses used for the experiments

	Wood specie	Dry composition						Humidity (w%)	LHV (MJ/kg)	Mean particle size (mm)
		C (w%)	H (w%)	O (w%)	N (w%)	S (w%)	Ashes (w%)			
Type A	Beech	48.3	6.7	44.4	0.11	<0.1	0.46	8.9	18.29	1
Type B	Resinous mix	52.3	7.2	40.1	0.09	<0.1	0.28	9.2	17.4	2
Type C	Resinous mix	49.9	7.1	42.4	0.12	<0.1	0.46	7.3	17.66	0.55
Type D	Beech	52.8	7.1	40.7	0.14	<0.1	0.29	9.3	18.3	0.3

Table 2: List of the experiments and their operating parameters

Oxidant	Oxidant flow	Feedstock	Temperature (°C)	Irradiation
H ₂ O	200 mg/min	Type A	1100	Direct
H ₂ O	200 mg/min	Type A	1150	Direct
H ₂ O	200 mg/min	Type A	1200	Direct
H ₂ O	200 mg/min	Type A	1300	Direct
H ₂ O	200 mg/min	Type A	1400	Direct
H ₂ O	500 mg/min	Type A	1100	Direct
H ₂ O	500 mg/min	Type A	1200	Direct
H ₂ O	500 mg/min	Type A	1300	Direct
H ₂ O	500 mg/min	Type A	1400	Direct
H ₂ O	200 mg/min	Type A	1100	Indirect
H ₂ O	200 mg/min	Type A	1150	Indirect
H ₂ O	200 mg/min	Type A	1200	Indirect
H ₂ O	200 mg/min	Type B	1100	Direct
H ₂ O	200 mg/min	Type B	1200	Direct
H ₂ O	200 mg/min	Type B	1300	Direct
H ₂ O	200 mg/min	Type B	1300	Direct
H ₂ O	200 mg/min	Type C	1200	Direct
H ₂ O	200 mg/min	Type C	1300	Direct
H ₂ O	200 mg/min	Type D	1100	Direct
H ₂ O	200 mg/min	Type D	1200	Direct
H ₂ O	200 mg/min	Type D	1300	Direct
H ₂ O (delayed)	200 mg/min	Type A	1200	Direct
H ₂ O (delayed)	200 mg/min	Type A	1300	Direct
CO ₂	0.2 NL/min	Type A	1100	Direct
CO ₂	0.2 NL/min	Type A	1200	Direct
CO ₂	0.2 NL/min	Type A	1300	Direct
CO ₂	0.2 NL/min	Type A	1400	Direct
CO ₂	0.6 NL/min	Type A	1200	Direct
CO ₂	0.6 NL/min	Type A	1300	Direct
CO ₂	0.6 NL/min	Type A	1400	Direct
CO ₂	0.2 NL/min	Type B	1100	Direct
CO ₂	0.2 NL/min	Type B	1200	Direct
CO ₂	0.2 NL/min	Type B	1300	Direct
CO ₂	0.2 NL/min	Type D	1200	Direct
CO ₂	0.2 NL/min	Type D	1300	Direct
CO ₂ (delayed)	0.2 NL/min	Type A	1300	Direct

Table 3: Comparison of the quantity of gas obtained from steam gasification (200 mg/min) in the directly and indirectly-irradiated reactor.

Temperature	Heating configuration	Production (mmol/g _{biomass})				Total	Cold Gas Efficiency
		CO	CO ₂	CH ₄	H ₂		
1100°C	Direct	22.05	3.79	5.21	22.70	53.75	0.90
	Indirect	22.46	5.75	6.89	24.99	60.08	1.02
1150°C	Direct	23.34	3.90	4.43	26.73	58.40	0.94
	Indirect	24.47	4.58	8.98	23.28	61.31	1.12
1200°C	Direct	25.81	3.64	2.21	31.69	63.35	0.96
	Indirect	25.94	4.74	8.04	27.22	65.94	1.15

Table 4: Calculated thermodynamic equilibrium composition of the syngas obtained at 1300°C (similar results were obtained at 1200°C and 1400°C)

Low CO ₂ flow rate (0.2 NL/min)		High CO ₂ flow rate (0.6 NL/min)	
CO	55.09 %mol	CO	56.25 %mol
H ₂	44.89 %mol	H ₂	31.06 %mol
Other	< 0.02 %mol	H ₂ O	7.82 %mol
		CO ₂	4.83 %mol
		Other	< 0.05 %mol

Table 5: Quantities of gas produced during steam gasification at different biomass feeding rates (same total amount injected: 10 g)

	Quantity of gas produced (mmole)					Total
	CO	H ₂	CO ₂	CH ₄	C _n H _m	
Low feed rate	228.7	287.0	41.3	19.8	2.0	578.8
High feed rate	248.1	307.2	26.9	17.0	1.4	600.6
Difference	7.85%	6.55%	-53.45%	-16.63%	-41.10%	3.63%

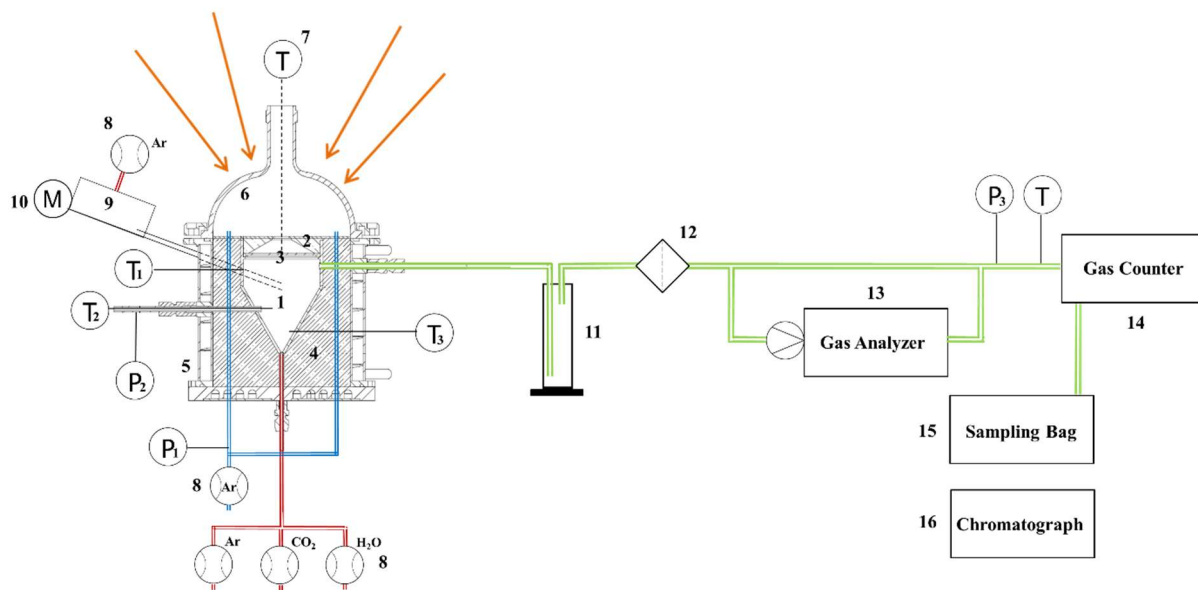


Figure 1: Experimental set-up: 1 Cavity; 2 Alumina cap; 3 Emissive plate; 4 Insulating material; 5 Cooled hull; 6 Window; 7 Pyrometer; 8 Gas and H₂O mass flow controller ; 9 Tilted hopper and feeding screw; 10 Driving motor; 11 Bubbler; 12 Cartridge filter; 13 In-line gas analyzer; 14 Gas volume counter; 15 Sampling bag; 16 Chromatograph

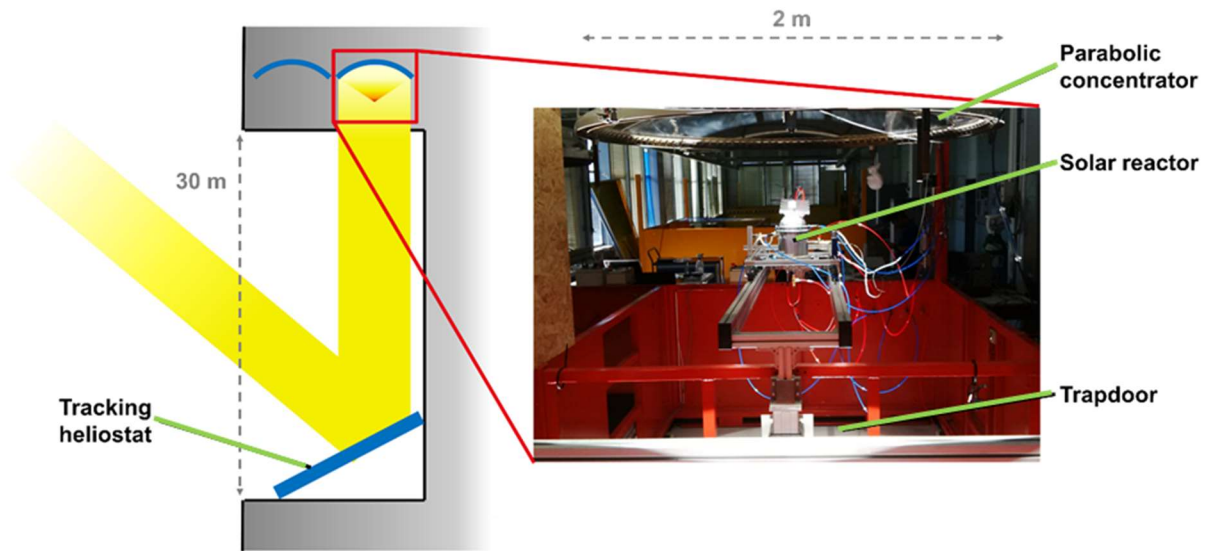


Figure 2: Solar reactor set-up at the CNRS-PROMES laboratory

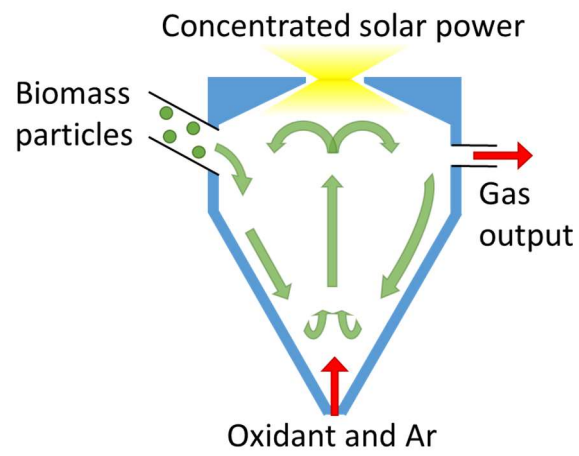


Figure 3: Particles trajectory in the reactor cavity

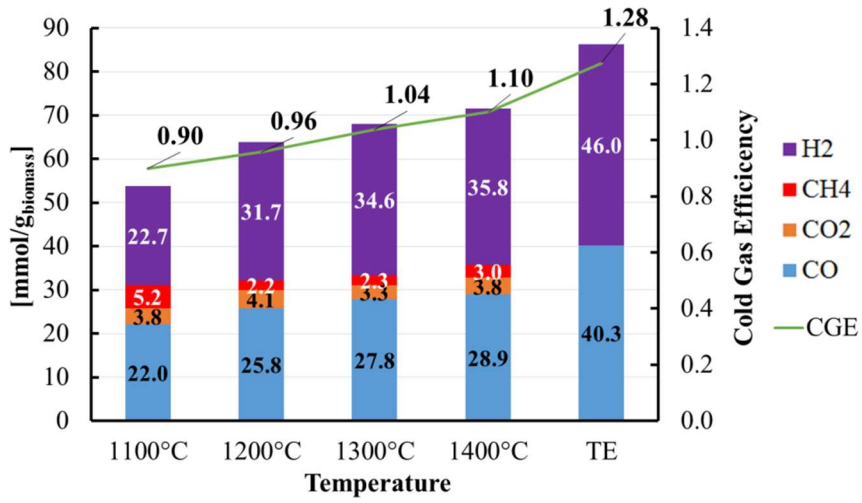


Figure 4: Comparison of the quantity of gas produced per gram of dry biomass during steam gasification (steam flow rate: 200 mg/min) at 1100°C, 1200°C, 1300°C and 1400°C and the evolution of the Cold Gas Efficiency.

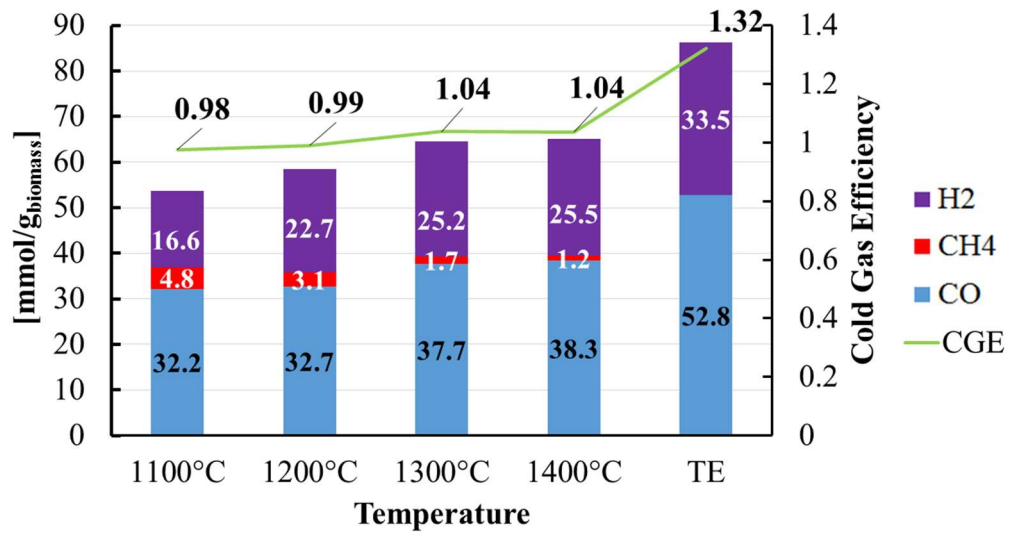


Figure 5: Comparison of the quantity of gas produced per gram of dry biomass during gasification with CO₂ (CO₂ flow rate: 0.2 NL/min) at 1100°C, 1200°C, 1300°C and 1400°C and the evolution of the Cold Gas Efficiency

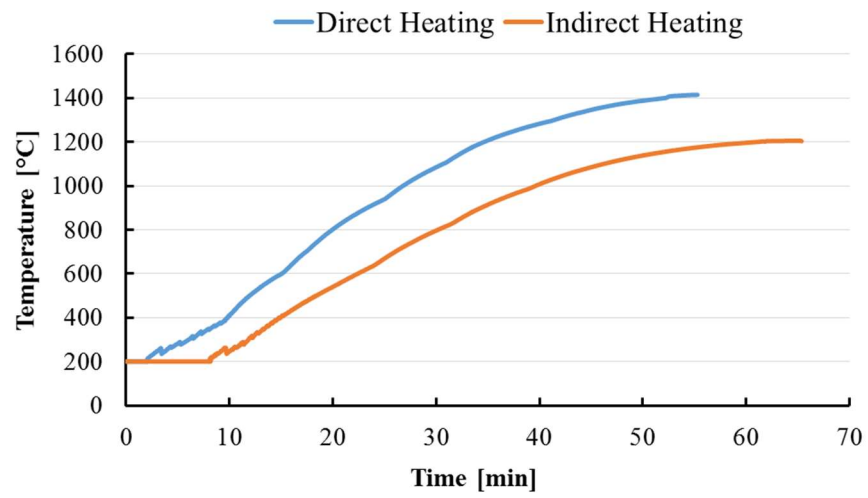


Figure 6: Evolution of the temperature (T_3) inside the cavity during heating phase

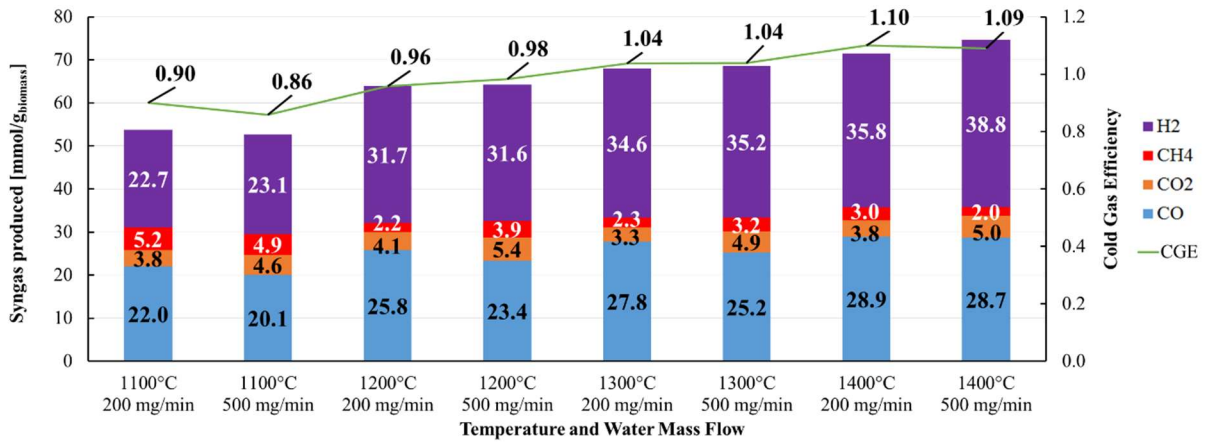


Figure 7: Influence of steam flow rate and temperature on syngas production.

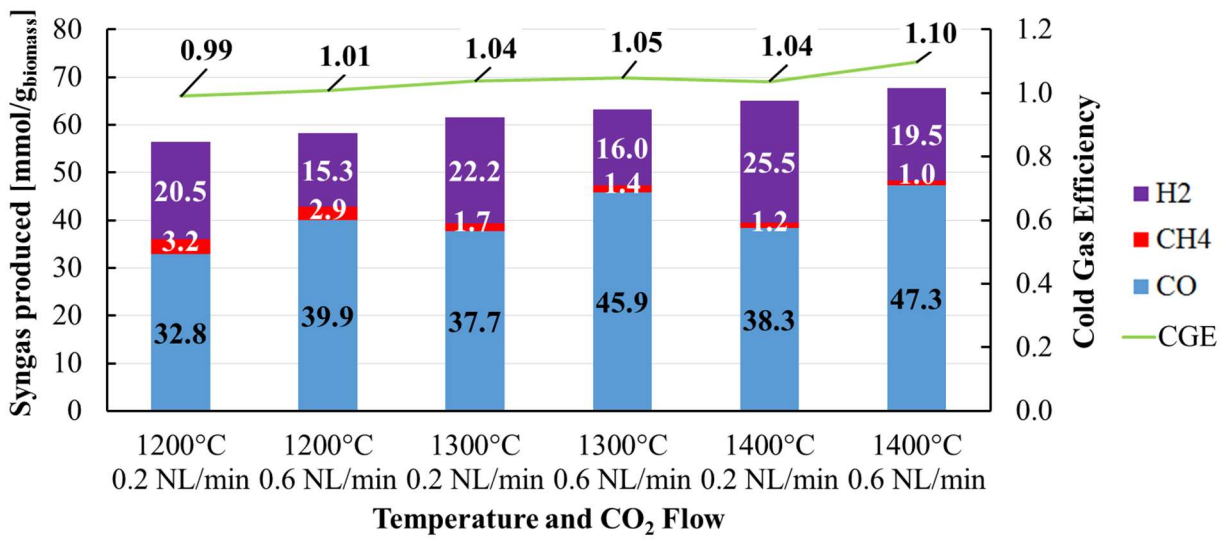


Figure 8: Influence of CO₂ flow rate (0.2 NL/min in 0.3 NL/min Ar-40% CO₂, and 0.6 NL/min-100% CO₂) and temperature on syngas production.

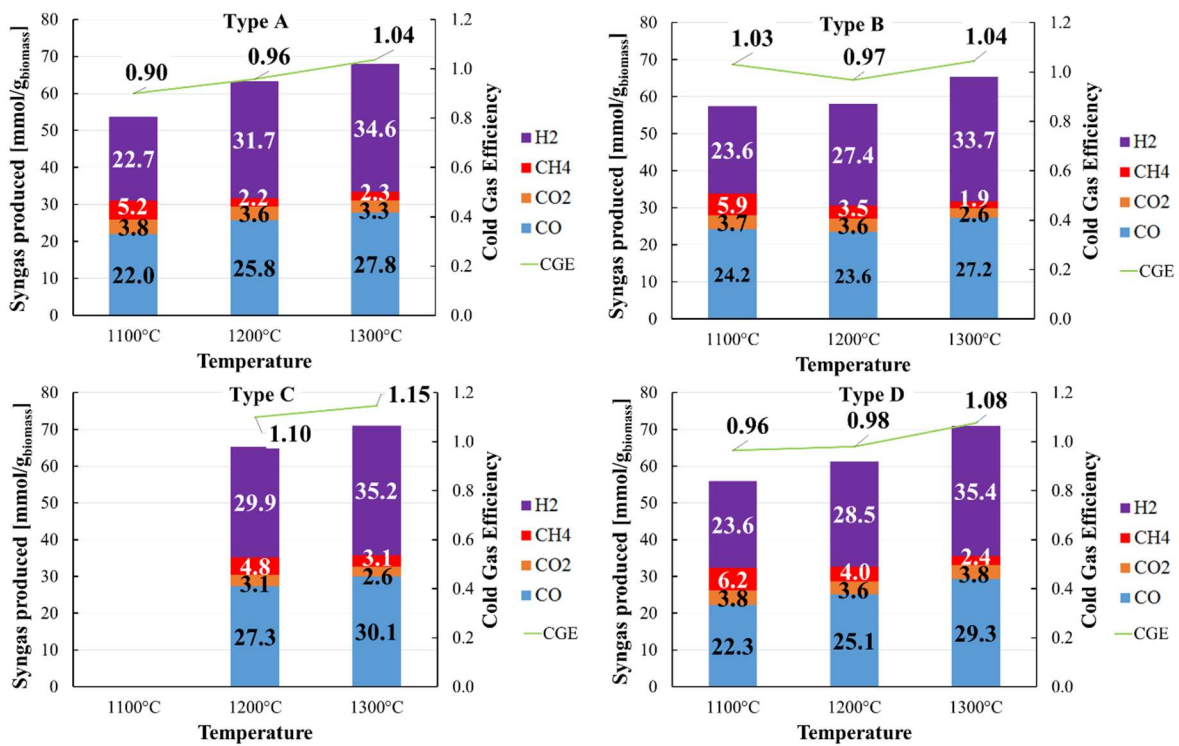


Figure 9: Quantity of gas produced during steam gasification (steam flow rate: 200 mg/min) of different types of feedstock

(Table 1)

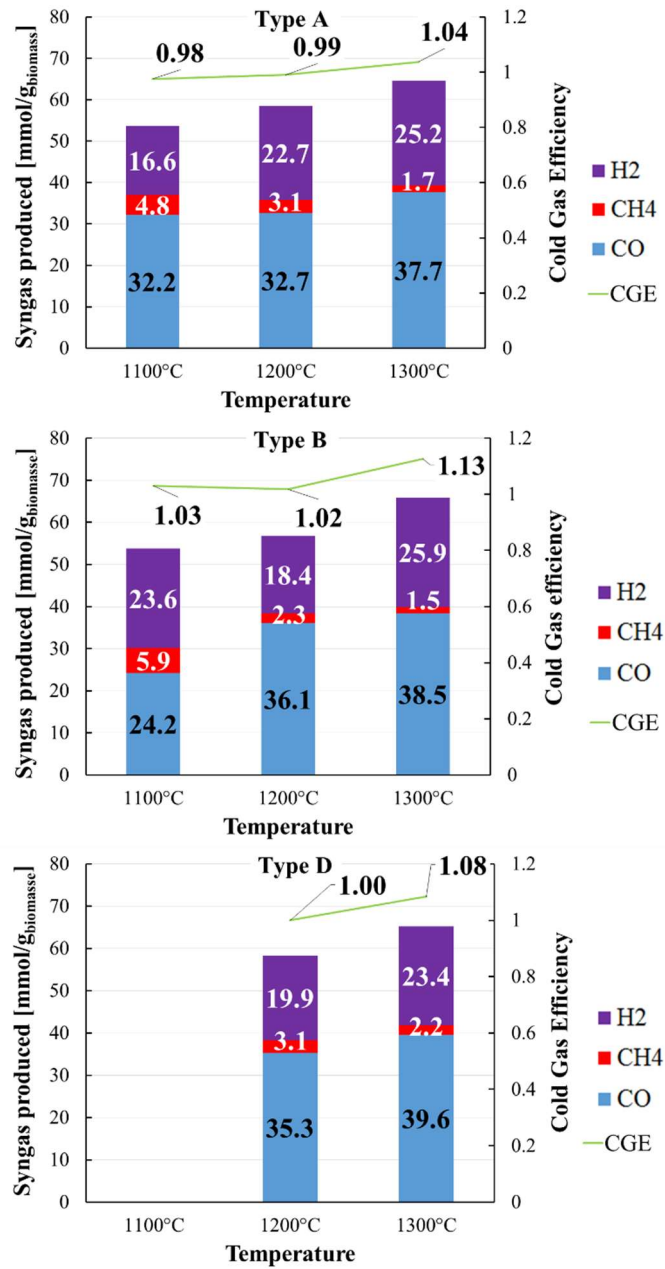


Figure 10: Quantity of gas produced during gasification with CO₂ (CO₂ flow rate: 0.2 NL/min) of different types of feedstock (Table 1)

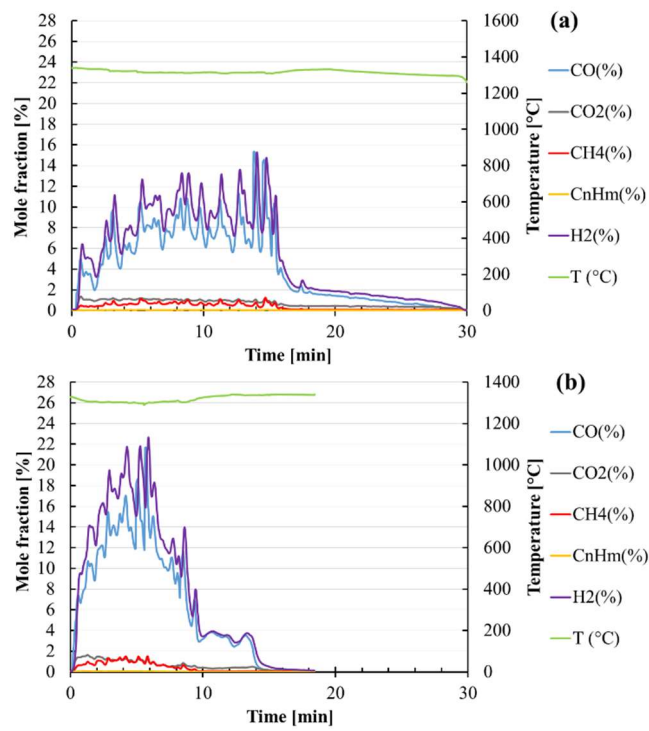


Figure 11: Influence of biomass feeding rate on gas species mole fraction during steam gasification at 1300°C for biomass feeding rates of (a) 0.65 g/min and (b) 1 g/min.

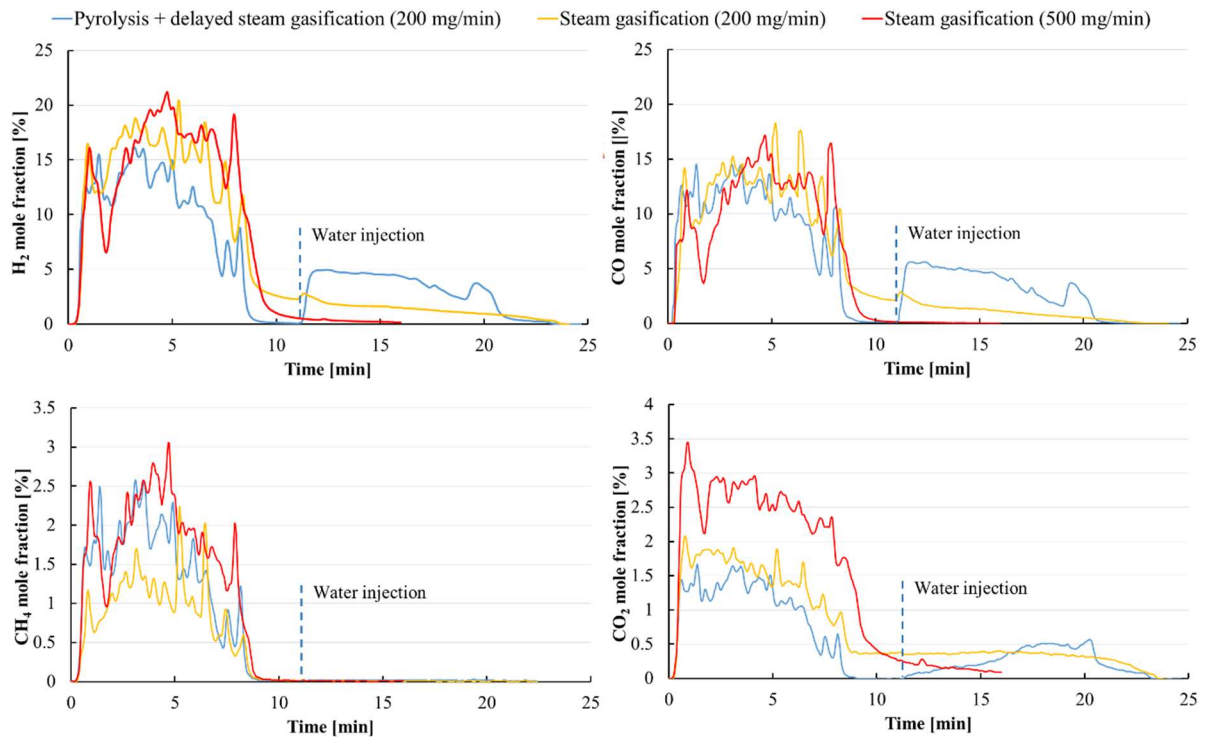


Figure 12: Comparison of the evolution of the mole fraction of H₂, CO, CO₂ and CH₄ in the syngas (argon included) during steam gasification (1300°C) at different steam flow rates and during pyrolysis with delayed steam injection.

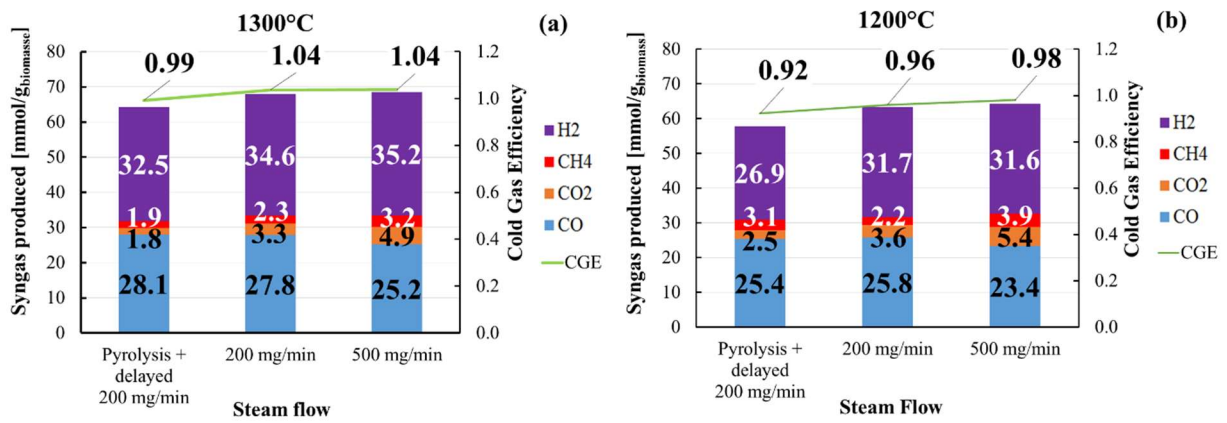


Figure 13: Comparison of the quantities of gas produced during steam gasification with continuous and delayed steam injection at 1300°C and 1200°C.

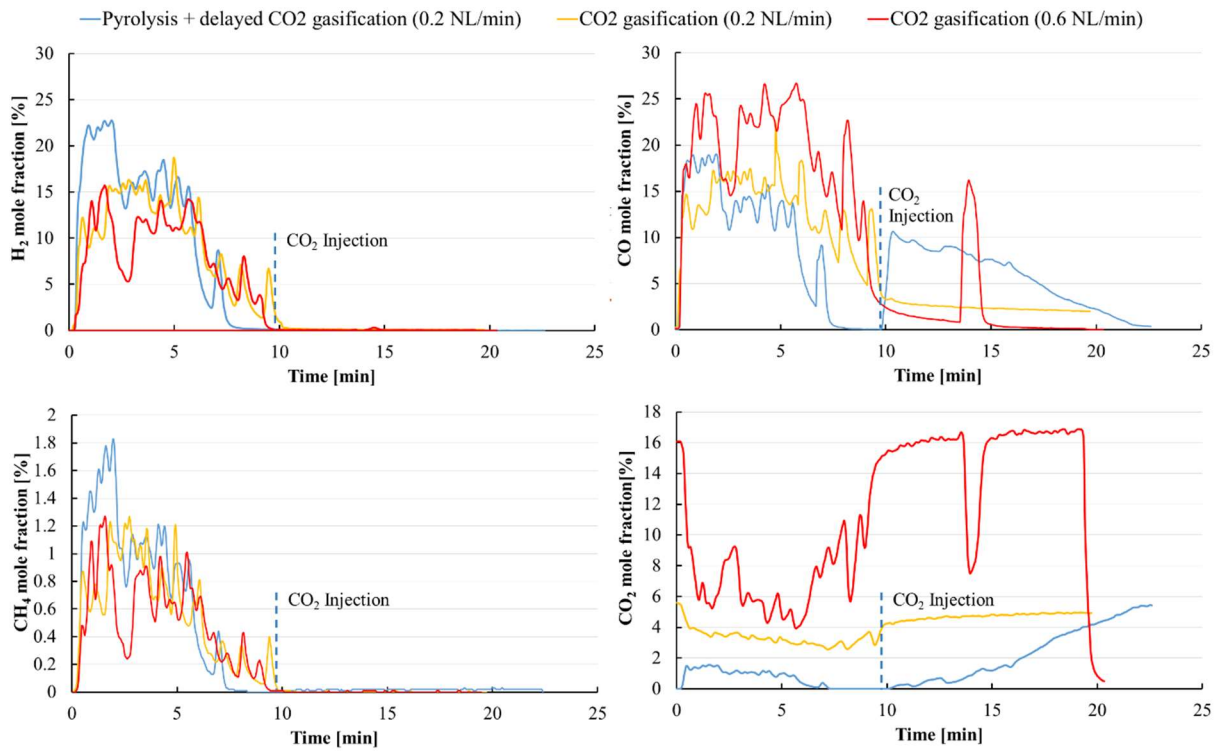


Figure 14: Comparison of the evolution of the mole fraction of H₂, CO, CO₂ and CH₄ in the syngas (argon included) during gasification with CO₂ (1300°C) at different CO₂ flow rates and during pyrolysis with delayed CO₂ injection.

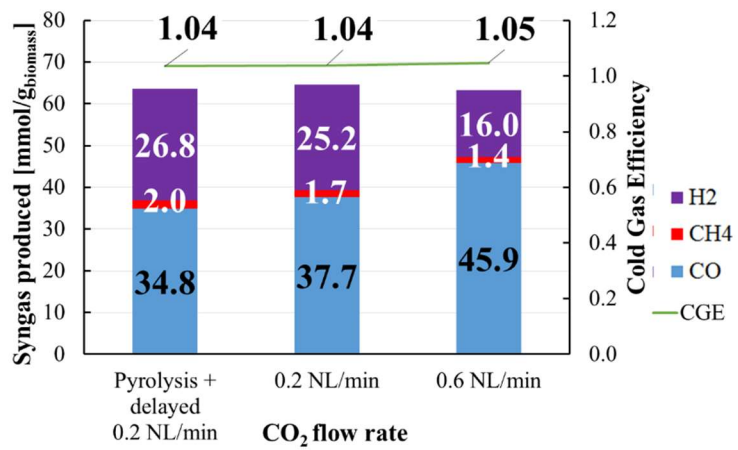


Figure 15: Comparison of the quantities of gas produced during gasification with CO₂ at 1300°C with continuous and delayed CO₂ injection